*A. P. Kfouri**

Elastic–Plastic Finite Element Analyses of Plates with Central Holes and Cracks under Biaxial Loading

REFERENCE Kfouri, A. P., **Elastic–plastic finite element analyses of plates with central holes and cracks under biaxial loading,** *Biaxial and Multiaxial Fatigue*, EGF 3 (Edited by M. W. Brown and K. J. Miller), 1989, Mechanical Engineering Publications, London, pp. 25–51.

ABSTRACT Results are presented of elastic–plastic finite element analyses of plates subjected to various biaxial stress states and containing either a circular or an elliptical central hole. Both cases have been further investigated for situations when cracks of two different lengths emanate from the central notch.

Three different stress states (uniaxial-, equibiaxial-, tension, and shear) are analysed for a material that corresponds to AISI 316 stainless steel by invoking the von Mises yield criterion, power law hardening and plane strain conditions. The development of notch plastic zones is illustrated and values of stresses and strains at notch roots are presented. When cracks are present, values of the CTOD, the J Integral, and G^{Δ} are compared for various stress–strain situations. The implications of the effects of biaxial modes of loading on fatigue crack propagation at notches are discussed and compared with analyses and experimental data from separate sources.

Introduction

The fatigue lifetime of engineering components and structures is frequently related to stress concentration fields created by notches. In a linear elastic material, the effect of such a field on the stress intensity factor, K, of a short crack emanating from the root of a notch has been studied by several workers, e.g., (**1**)–(**4**). For uniaxial elastic loading, the depth of the notch field effect, S, on K is small and is approximately given by

$$S = 0.13\sqrt{(D\varrho)} \tag{1}$$

where D is the depth and ϱ the root radius of the notch, respectively (**3**).

Even so, despite its small range, the notch field is important because the fatigue crack spends a large proportion of its life under this influence.

In the past decade there has been an increasing awareness of the limitations of linear elastic fracture mechanics (LEFM) when describing crack tip fields particularly at high stress levels, i.e., $\sigma_p/\sigma_{yo} > 0.4$ (see Notation, below) when small scale yielding (SSY) conditions do not apply. In such cases, elastic–plastic fracture mechanics (EPFM) must be used, and this is particularly true when cracks are situated in plastic enclaves located in notch roots. The aim of this

* Department of Mechanical Engineering, University of Sheffield, Mappin Street, Sheffield S1 3JO, UK.

present work is to understand the interaction of notch plasticity and crack tip plasticity using elastic–plastic finite element analyses. Of special interest is a study of the effect of biaxial stress states, notch profiles, and crack lengths. Geometrical configurations and elastic–plastic material properties were chosen to relate to biaxial fatigue crack propagation experiments on AISI 316 stainless steel carried out in the Department of Mechanical Engineering of the University of Sheffield (4).

Notation

a	Major axis of the elliptical hole
b	Minor axis of the elliptical hole
B	Non-dimensionalised T term
c	Nominal defect length
G	Griffith's energy release rate
G_N	Value of G for an Inglis crack of length $2c$
G^Δ	Crack separation energy rate
H	Half the length of a specimen
J	Value of J contour integral
K_I	Mode I stress intensity factor
K_t	Stress concentration factor
r	Distance from the tip of the crack
T	Elastic T term
v	Displacement of crack face
W	Half the side of the square plate
Y	Stress intensity geometry factor
Γ	Path of J contour integral
λ	Biaxial loading mode ($= \sigma_Q/\sigma_p$)
σ_p	Applied stress normal to the major axis of the ellipse or the crack
σ_Q	Applied stress parallel to the major axis of the ellipse or the crack
σ_y	Current yield stress
σ_{yo}	Initial yield stress

The analyses

Square plates (see Fig. 1) with sides of length $2W = 100$ mm and containing a central elliptical hole with major axis $a = 8$ mm and minor axis $b = ka$ (where $k = 0.5$ or 1.0), were subjected to edge stresses σ_p and σ_Q (a positive sign for tension) applied in directions normal to the major and minor axes of the ellipse, respectively. For each notch geometry three cases of crack length were considered, namely zero, 2 mm, and 4 mm, extending from the notch root along the major axis giving nominal overall defect lengths, c, equal to 8 mm, 10 mm, and 12 mm, respectively.

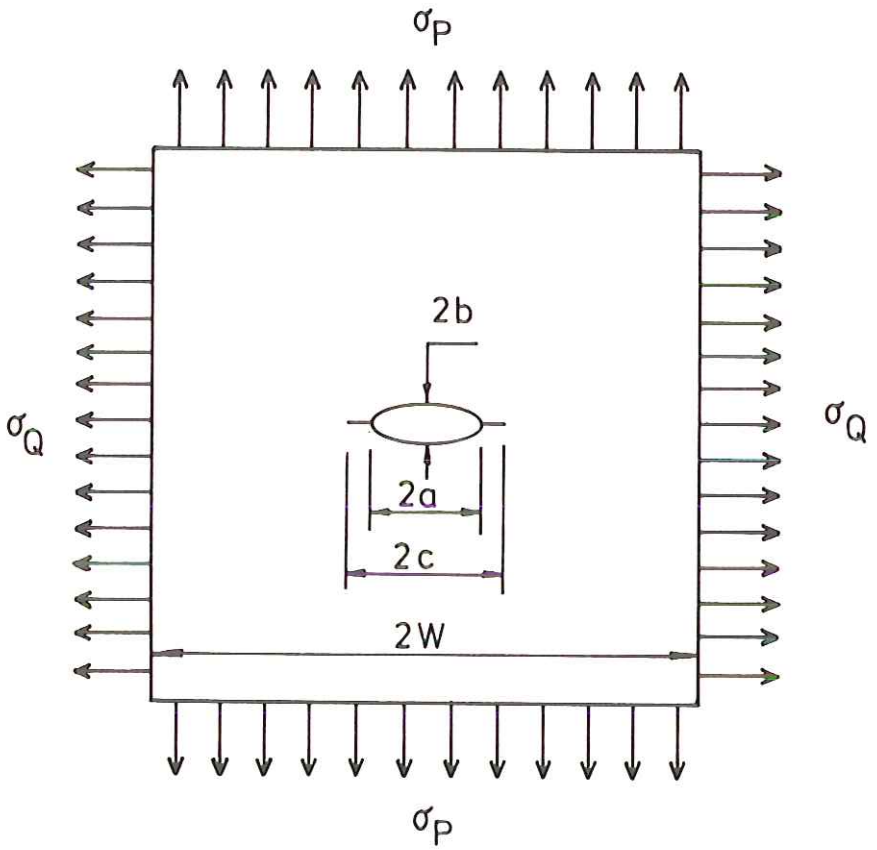

Fig 1 The 100 mm square plate with a central elliptical notch subjected to biaxial stress

A biaxial load was applied to each configuration, with the biaxiality parameter

$$\lambda = \frac{\sigma_Q}{\sigma_p} \tag{2}$$

having values of 0, 1, and −1. For the uniaxial ($\lambda = 0$) and equibiaxial ($\lambda = 1$) loading modes, the maximum value of σ_p was 280 MPa. For the shear mode ($\lambda = -1$) the maximum value of σ_p was 193 MPa. Comparison between all biaxial states was made at a value of σ_p equal to 193 MPa.

Plane strain elastic–plastic finite element analyses were performed, based on the Von Mises yield criterion, a modulus of elasticity equal to 198 000 MPa and an elastic Poisson's ratio of 0.29. Power law hardening was assumed, whereby the yield stress, σ_y, takes the largest of the two values: (i) σ_{yo}, or (ii) $579\bar{\varepsilon}_p^{0.064}$.

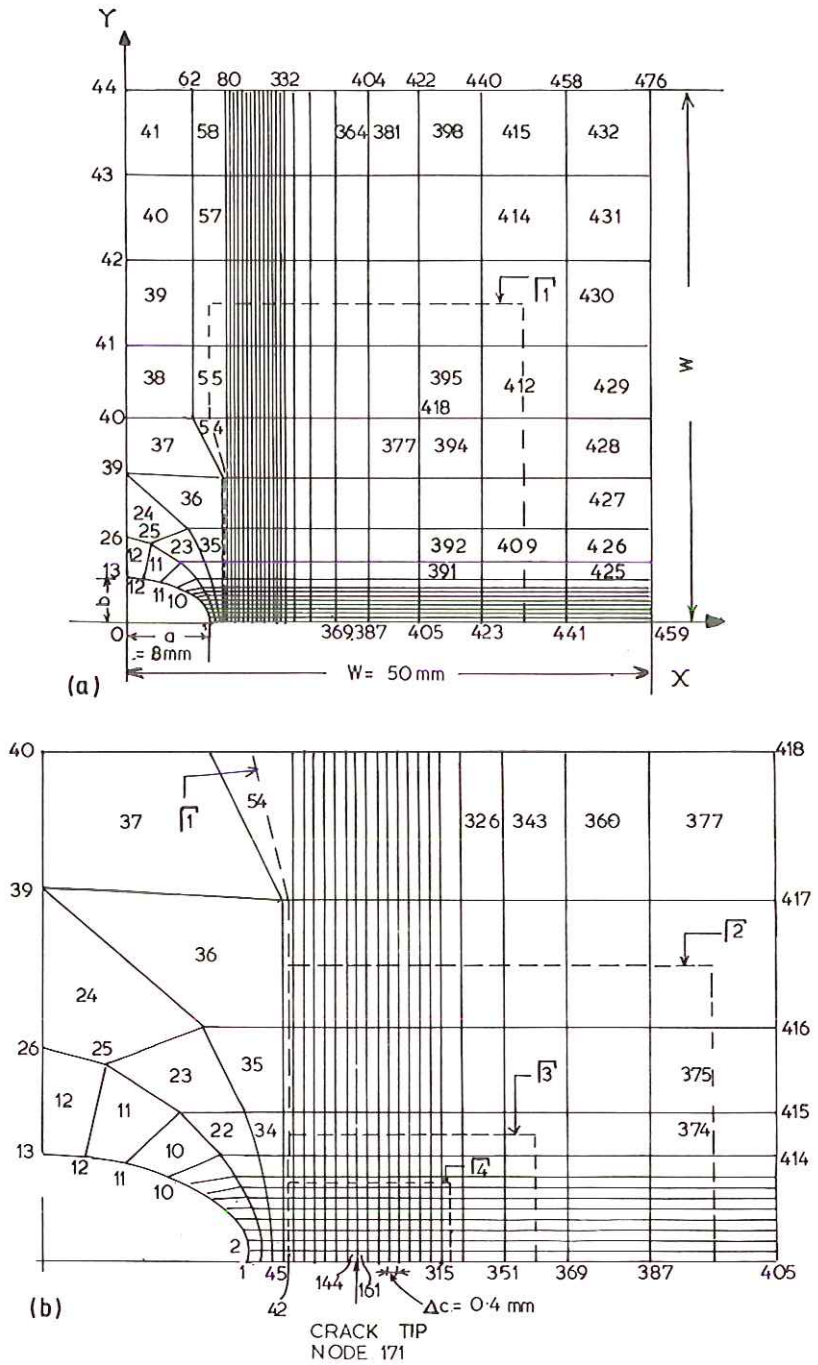

Fig 2 Upper right hand quadrant of the plate of Fig. 1; (a) finite element idealization showing the numbering of the elements, (b) magnification of the region near the notch tip. Paths for the *J* contour integral evaluations are also shown

Here σ_{yo} (= 320 MPa) is the initial yield stress, and $\bar{\varepsilon}_p$ is the equivalent plastic strain.

A typical finite element idealization of a quadrant of the plate is shown in Fig. 2(a), and in the analysis advantage was taken of the symmetry of the configuration. A magnified view of the region near the crack tip and the notch is also shown, in Fig. 2(b), which corresponds to the case $k = 0.5$ and $c = 12$ mm. The numbers of some of the nodes and of the 'linear strain' isoparametric quadrilateral elements are indicated as are the four paths of the J contour integrals Γ_1, Γ_2, Γ_3, and Γ_4. For the shorter 2 mm crack, the paths come close to the crack tip. This could reduce the accuracy of the J integrals because of the high stress gradients in the vicinity of the crack tip. In all cases the initial load σ_{po} was adjusted automatically to 0.95 times the value of σ_p required to cause incipient yielding so that the first response was entirely elastic. This was followed by an incremental elastic–plastic analysis. At various levels of the load, information was obtained concerning stresses and strains, plastic zone sizes, crack tip opening displacements (CTODs), crack profiles, J integrals, and crack separation energy rates, G^{Δ}.

The results

A check on the elastic analyses was obtained by calculating the stress concentration factors, K_t, for the central holes without cracks. These are given in Table 1 for the two aspect ratios considered here. The results are approximate since the element stresses were obtained at the centres of the elements and these were extrapolated to the notch boundary. Comparisons in Table 1 are made with classical analytical solutions for an infinite plate and also Peterson's

Table 1 Comparisons of stress concentration factors, K_t, for an elliptical hole, of various aspect ratios, in plates of different geometry

Notch ratio b/a	*Plate geometry* a/W	H/W	Biaxial stress state $\lambda = 0$	$\lambda = 1$	$\lambda = -1$	*Source*
			Stress concentration factor			
1.0	0	1	3	2	4	EAS
	0.16	1	3.28	2.11	4.46	PFES
	0.16	∞	3.09	–	–	REP
0.5	0	1	5	4	6	EAS
	0.16	1	5.05	4.07	6.04	PFES
	0.16	∞	5.12	–	–	REP

Sources
EAS – Exact analytical solution for an infinite plate.
PFES – the present finite element solution.
REP – R. E. Peterson (**5**), $a/W = 0.16$.

solution (**5**) for a long plate with finite width. Note that the ratio $K_t(\lambda = -1)/K_t(\lambda = 1)$ is approximately 2 for the circle, but only 1.5 for the ellipse.

Turning now to cracked notches, Table 2(a) presents stress intensity geometry factors, Y, determined from the present analysis for a/W equal to 0.16 and H/W equal to unity. The Y factors were derived from both J integral and G^{Δ} values, the latter using a crack tip release technique. It will be recalled that $G^{\Delta} = \Delta E/\Delta c$, where ΔE is the crack surface separation energy absorbed during a small finite crack growth step, Δc (**6**)(**7**). When the material is linear elastic, G^{Δ} is equal to Griffith's energy release rate, G.

Since the data in Table 2(a) is compared with the infinitely long plate results of reference (**1**), Table 2(b) has been included in order to compare Y values for a centrally cracked (but unnotched) plate when $H/W = 1$ and when $H/W = \infty$;

Table 2 Comparisons of stress intensity geometry factors, Y, obtained using different methods, for $a/W = 0.16$ (a) for a crack emanating from an elliptical hole, (b) for a plane crack with different values of H/W using Isida's and finite element results based on J

(a)

Notch ratio b/a	*Defect ratio* c/W	*Plate ratio* H/W	*Biaxiality ratio* $\lambda = 0$	$\lambda = 1$	$\lambda = -1$	*Source*
			Stress intensity Y *factor*			
1	0.2	>2.0	1.072	0.857	1.290	XBM
	0.2	1.0	1.075	0.810	1.359	J
	0.204	1.0	1.124	0.850	1.399	G^{Δ}
	0.25	>2.0	1.121	0.944	1.254	XBM
	0.24	1.0	1.157	0.953	1.372	J
	0.244	1.0	1.181	0.977	1.384	G^{Δ}
0.5	0.2	>2.0	1.064	0.987	1.143	XBM
	0.2	1.0	1.066	0.977	1.163	J
	0.204	1.0	1.111	1.013	1.208	G^{Δ}
	0.25	>2.0	1.077	1.046	1.111	XBM
	0.24	1.0	1.100	1.045	1.161	J
	0.244	1.0	1.123	1.063	1.182	G^{Δ}

Sources
XBM – S. T. Xiao, M. W. Brown, and K. J. Miller (**1**).
J – J derivation.
G^{Δ} – G^{Δ} derivation.

(b)

Defect ratio c/W	*Plate geometry* H/W = *1*	H/W > *2*	*Ratio* H/W = *1* / H/W > *2*	Y *from* J *when* H/W = *1*
	Y *factors**			
0.2	*1.055*	*1.025*	*1.029*	*1.044*
0.3	*1.123*	*1.060*	*1.059*	*1.111*

* *M. Isida* (**8**).

reference (8). The values of Y obtained from J evaluations using a comparable finite element mesh to the one used in the present paper are also shown in Table 2(b) and are approximately 1 per cent lower than the Isida figures.

Thus, by applying a correction factor of 1.029 to the values of $Y = 1.072$ and $Y = 1.064$ in Table 2(a) that correspond to the two different notches with $c/W = 0.2$, $\lambda = 0$, and $H/W = \infty$, one obtains 'corrected' values of Y equal to 1.103 and 1.095, respectively. These values are in reasonable agreement with values of 1.113 and 1.100, respectively, obtained from G^{Δ} calculations, when allowing for appropriate adjustment for the slightly shorter crack length of 0.2 mm. The Y values obtained from J evaluations are also in reasonable agreement when considering the larger crack length of 4 mm, but appear somewhat low for the shorter 2 mm crack.

The results of the elastic–plastic finite element analyses are presented in Figs 3–14. Figures 3–8 show the plastic zones for different geometries, load levels, and biaxial stress states. Figure 3 refers to the plate with the circular hole without a crack, while Figs 4 and 5 refer to the circular hole with 2 mm and 4 mm cracks, respectively. Figure parts (a), (b), and (c) correspond to $\lambda = 0, \lambda = 1$, and $\lambda = -1$. In addition, Fig. 4(d) shows the plastic zone after two crack growth steps for the same loading pattern as in Fig. 4(b). Figures 6, 7, and 8 show the plastic zones for the plate with the elliptical hole.

From the finite element analyses much useful data is gained concerning concentration factors at notch roots in elastic–plastic materials. Figure 9 provides information on the variation of principal stresses at the centre of the element and equivalent strains averaged over the element exhibiting the maximum values for each of these parameters, respectively, as a function of the applied load, for each of the three biaxial stress modes studied. However, these values of principal stresses and equivalent strains are mainly of a qualitative nature, for reasons which will be explained later.

Figure 10 illustrates crack flank profiles for various applied stress levels, two crack lengths, two notch profiles, and three biaxial stress ratios.

Figure 11 displays the relationship between the J contour integral and the CTOD, normalized with respect to Δc, i.e., calculated as $2000\, v/\Delta c$, where v is the displacement normal to the crack plane, of the node on the crack flank behind the crack tip node, and Δc is the distance separating the two aforementioned nodes.

Figure 12 shows, for the different conditions indicated, values of J (evaluated on path Γ_3) normalized with respect to G_N, where G_N is Griffith's energy release rate for an Inglis crack of length $2c$ given by

$$G_N = \sigma_p^2 \pi c (1 - \nu^2)/E \tag{3}$$

against a measure of the applied load given by $(\sigma_p/\sigma_{yo})^2$.

Using a similar measure of applied load for the two cracked configurations, Fig. 13 shows, for different biaxial stress states, the maximum values of equivalent strains averaged across the most deformed crack tip element, i.e., the element behind the crack tip.

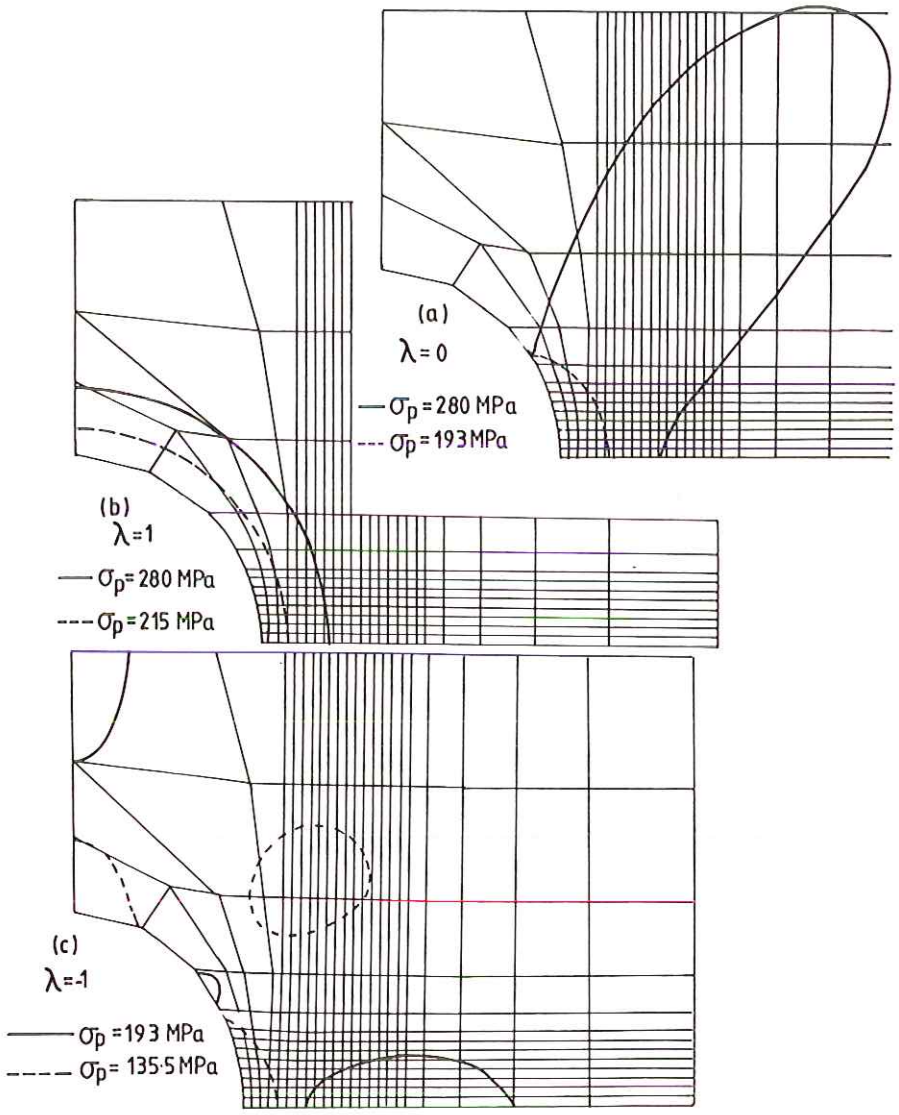

Fig 3 Plastic zones round the circular hole for the different loading modes: (a) $\lambda = 0$, (b) $\lambda = 1$, (c) $\lambda = -1$. Note $\sigma_Q = \lambda\sigma_P$

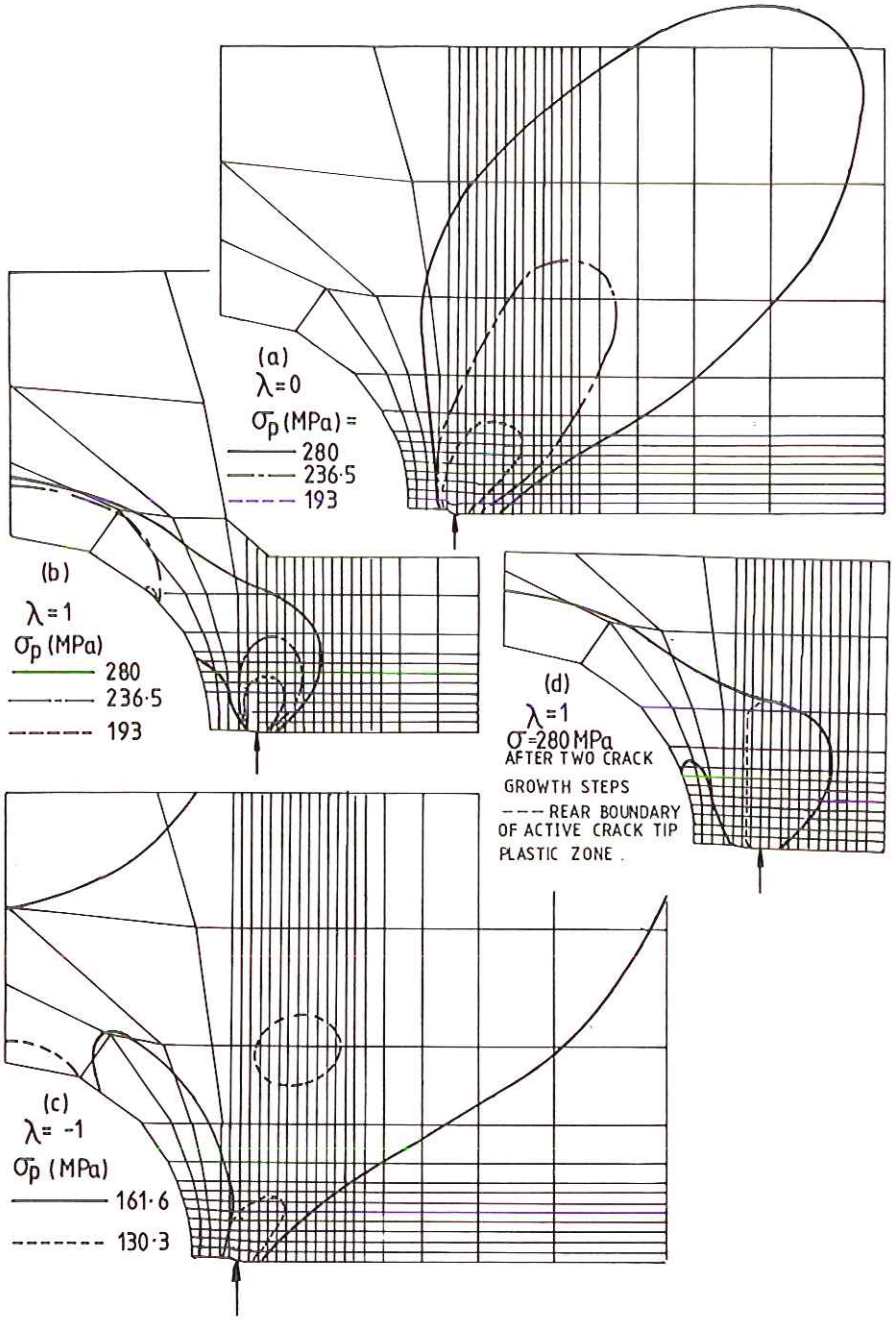

Fig 4 Plastic zones at the tip of 2 mm cracks emanating from the circular hole of Fig. 3. Loading modes: (a), (b), (c) as in Fig. 3, (d) after two crack growth steps with σ_Q and $\sigma_p = 280$ MPa

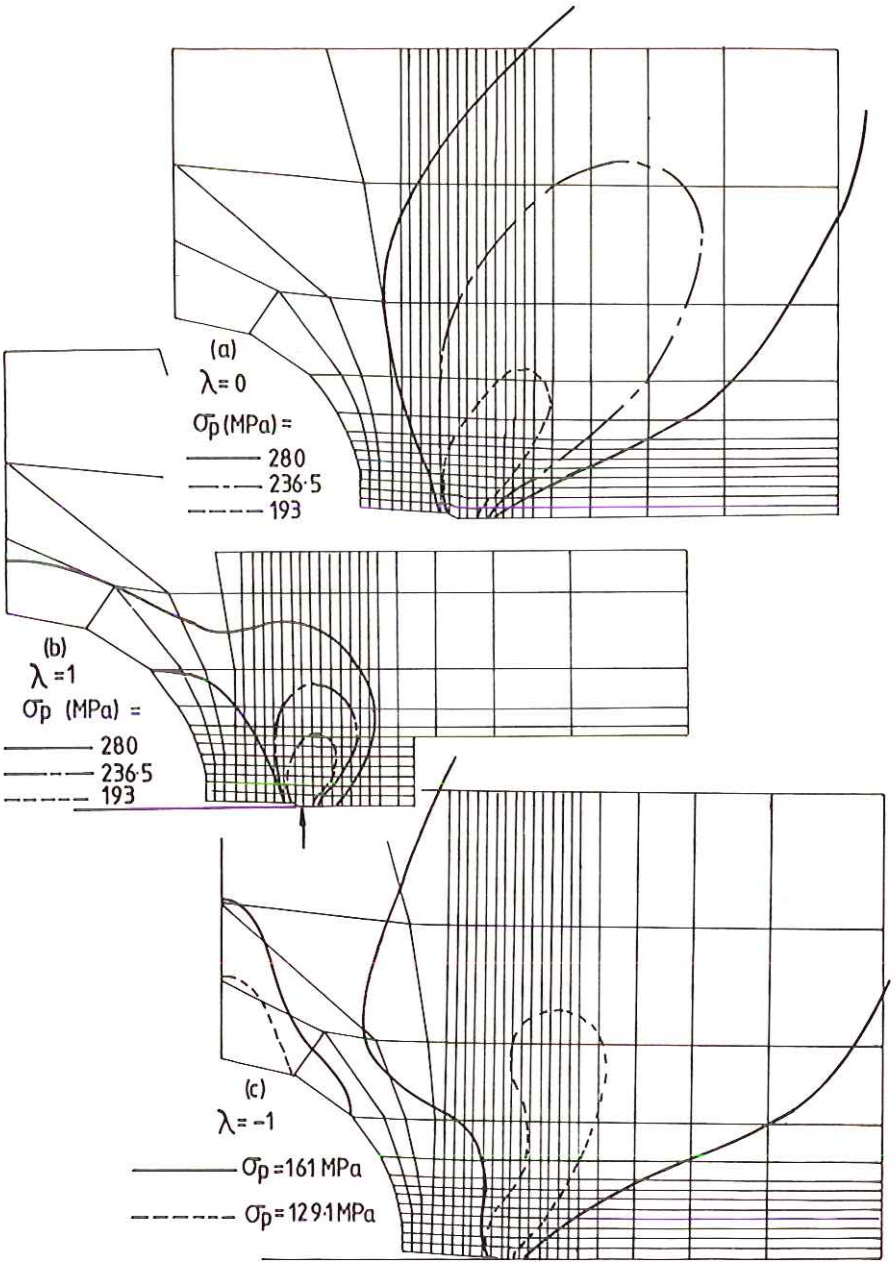

Fig 5 Plastic zones at the tip of 4 mm cracks emanating from the circular hole of Fig. 3. Loading modes: (a), (b), (c) as in Fig. 3

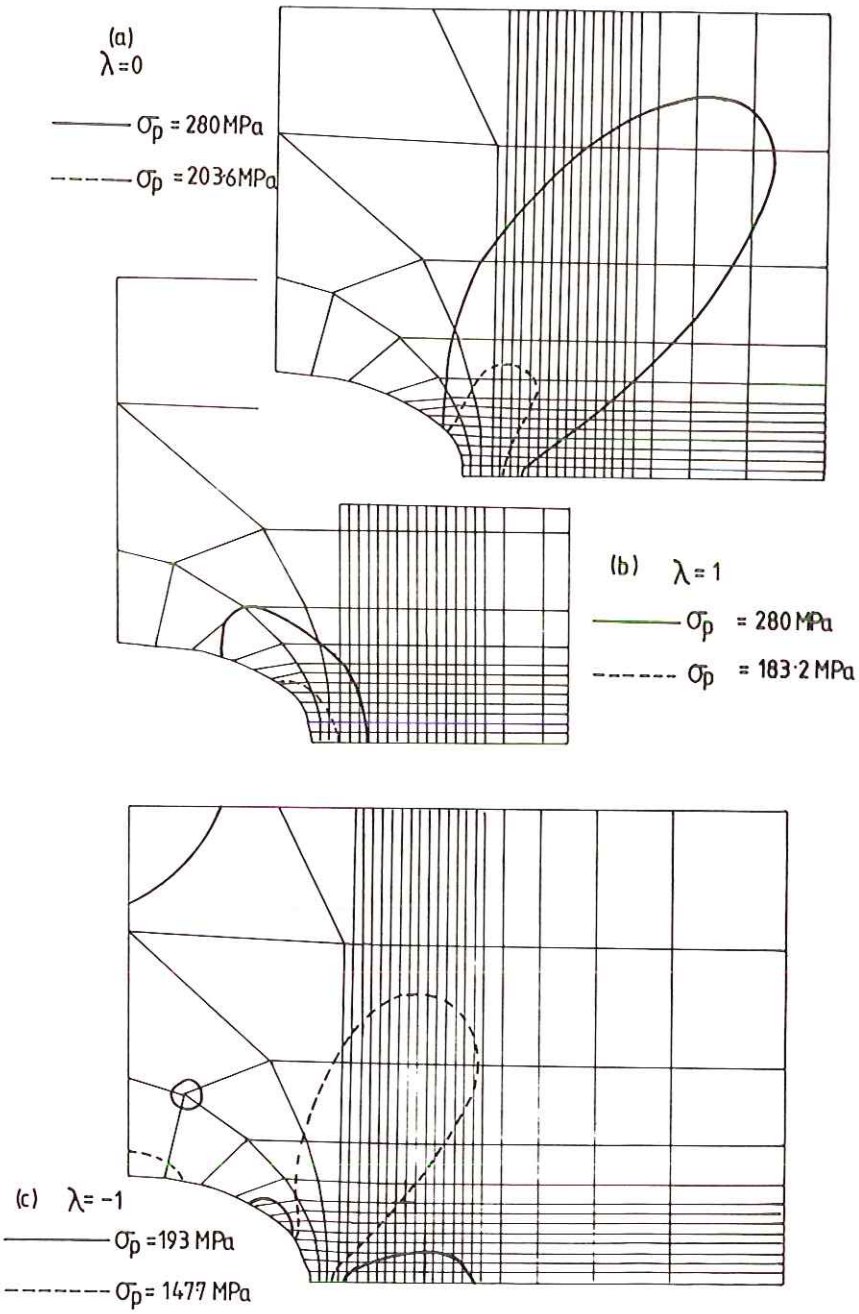

Fig 6 Plastic zones for the elliptical hole for the different loading modes: (a) $\lambda = 0$, (b) $\lambda = 1$, (c) $\lambda = -1$. Note $\sigma_Q = \lambda\sigma_p$

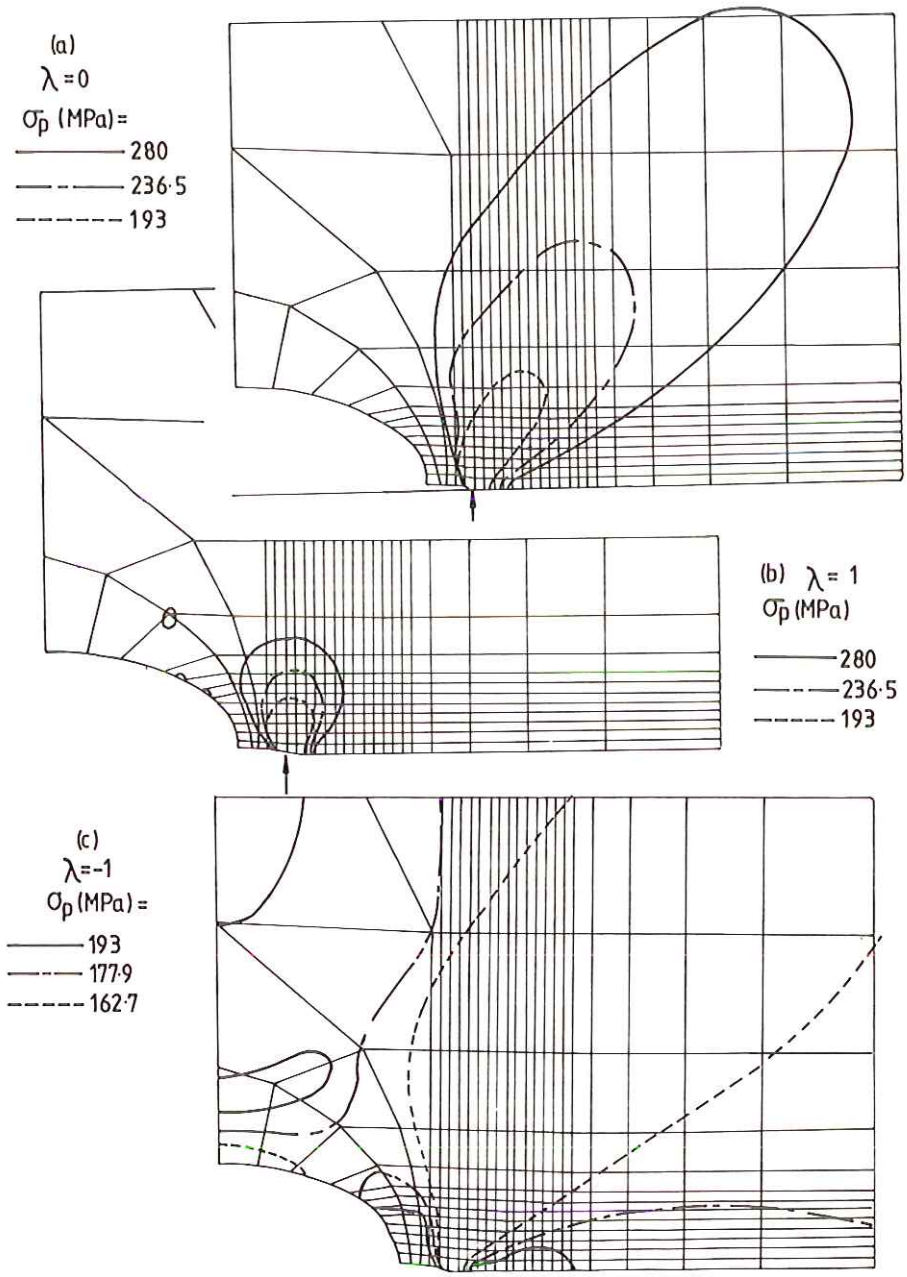

Fig 7 Plastic zones at the tip of 2 mm cracks emanating from the elliptical hole of Fig. 6. Loading modes: (a), (b), (c) as in Fig. 6

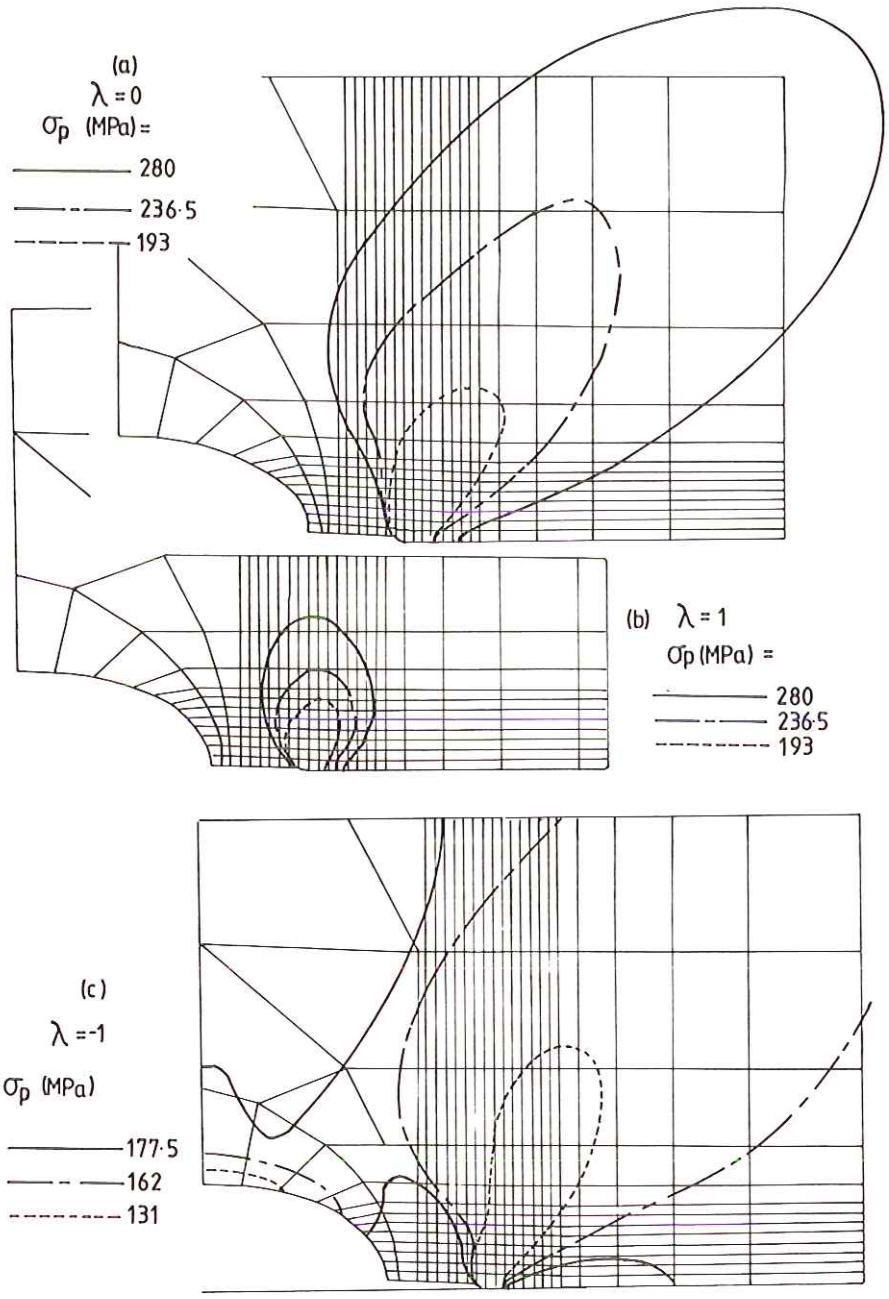

Fig 8 Plastic zones at the tip of 4 mm cracks emanating from the elliptical hole of Fig. 6. Loading modes: (a), (b), (c), as in Fig. 6

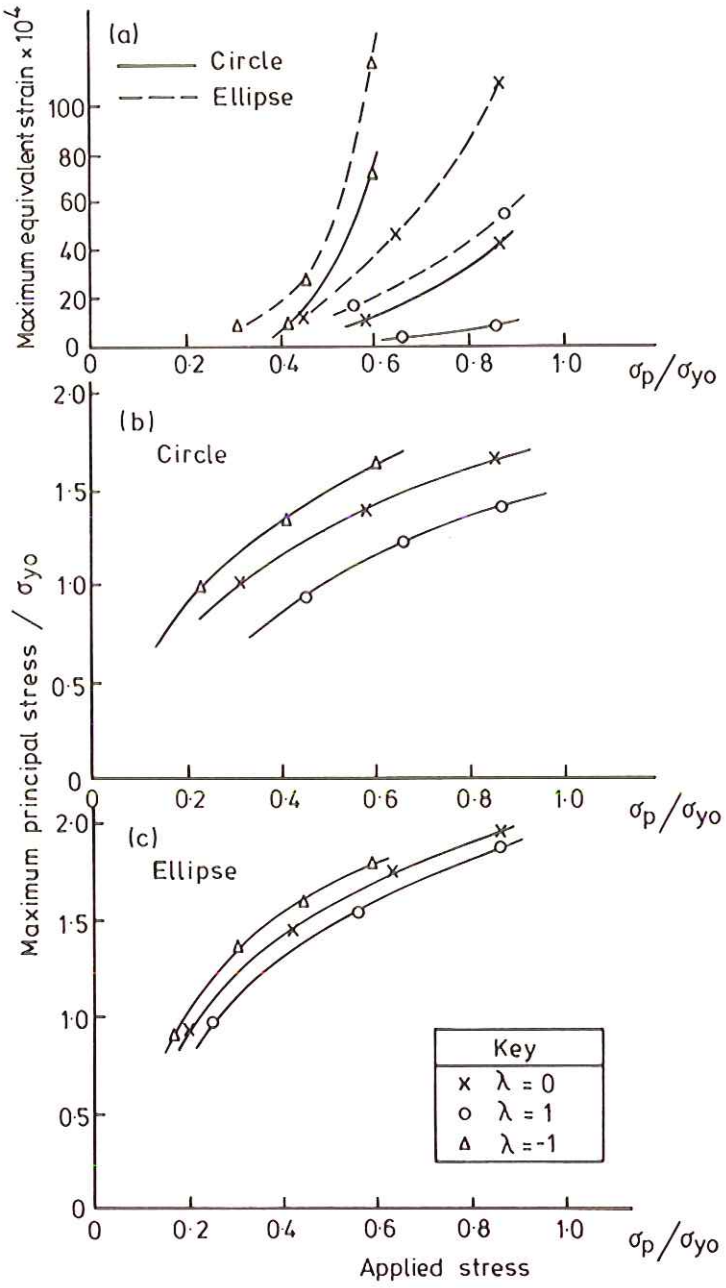

Fig 9 Variation of stresses and strains at notch roots: (a) equivalent plastic strain in the most highly strained element, averaged over the element for the plate with the circular hole (solid line) and the elliptical hole (broken line), (b) largest normalised principal stress at the centres of the elements, against the normalised applied stress, for the plate with the circular hole, (c) as (b), but for the plate with the elliptical hole

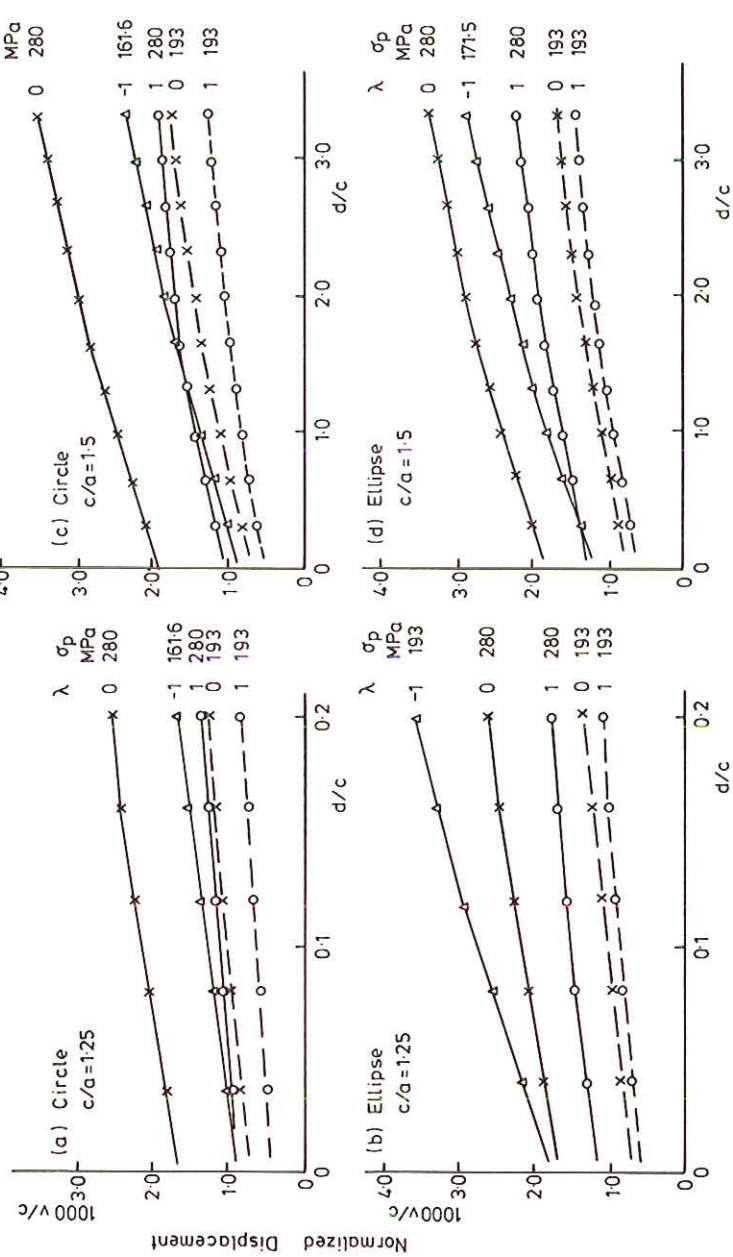

Fig 10 Crack profiles showing the normalised displacement against the normalised distance from the crack tip, for cracks emanating from circular and elliptical holes

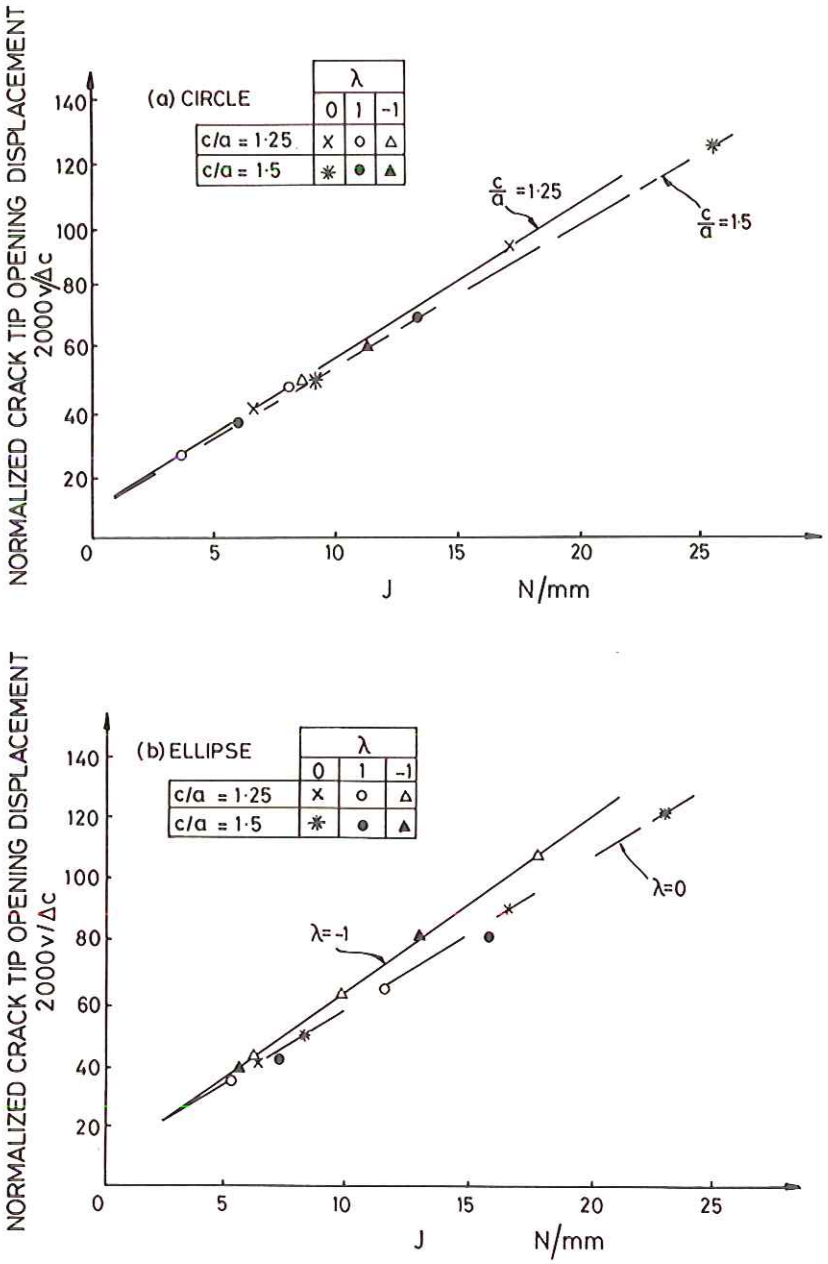

Fig 11 Crack tip opening, against J, for the plate with: (a) the circular hole, (b) the elliptical hole

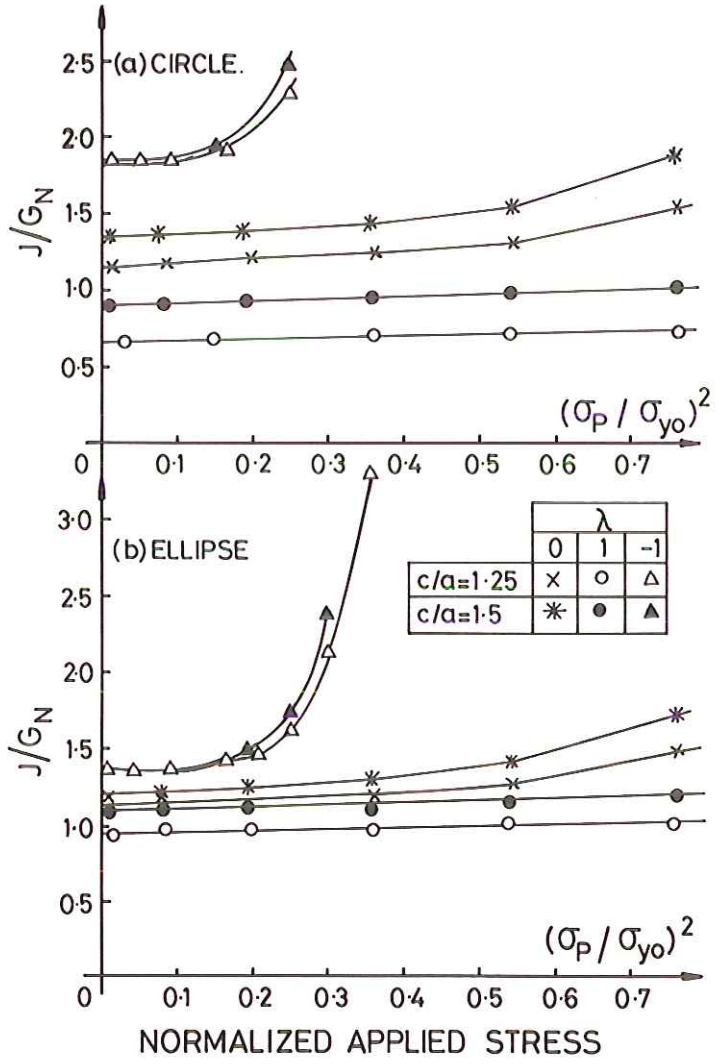

Fig 12 Normalised values of the contour integral, against the normalised applied stress, for the crack lengths and the loading modes indicated: (a) the circular hole, (b) the elliptical hole

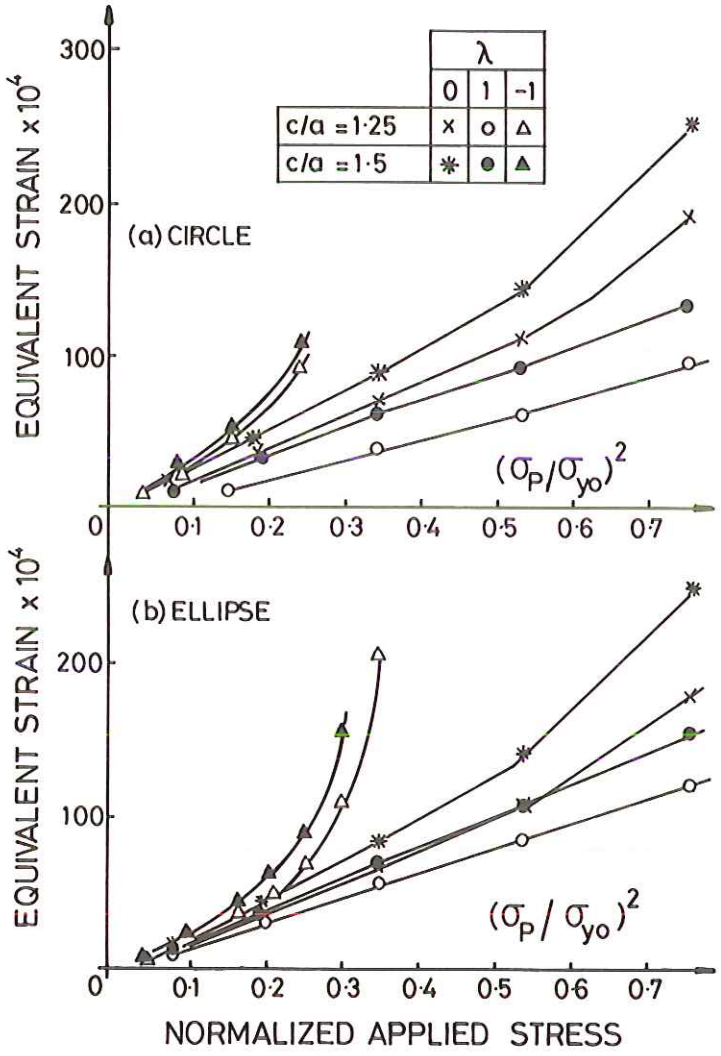

Fig 13 Equivalent average plastic strain in the crack tip element against the normalised load, for the crack lengths and the loading modes indicated: (a) the circular hole, (b) the elliptical hole

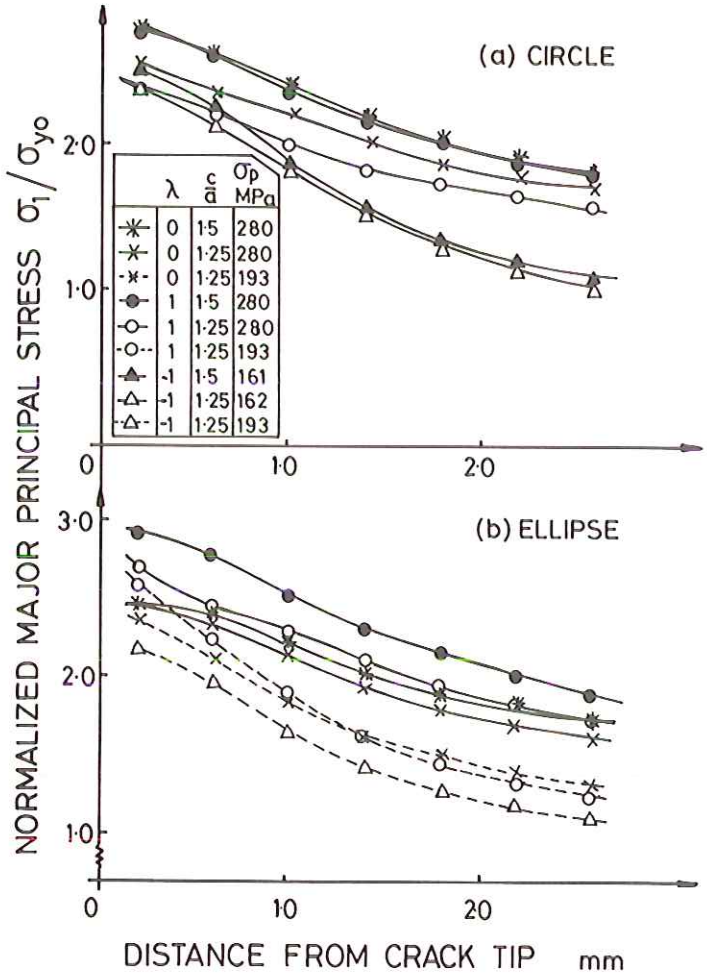

Fig 14 Normalised major principal stresses at the centres of the elements on the crack plane against the horizontal distance ahead of the crack tip: (a) the circular hole, (b) the elliptical hole

Finally, Fig. 14 plots the variation of the principal stress at the centre of the elements ahead of the crack tip as a function of the distance ahead of the tip.

Discussion

Plastic zones and concentration factors at uncracked notches

From Fig. 3 and Fig. 6 it is clear that a major effect on the development of plastic zones is due to the parameter λ. For the uniaxial mode, $\lambda = 0$, the zones are not dissimilar in shape to crack tip plastic zones developed in cracked bodies (Figs 4(a), 5(a), 7(a), and 8(a)); this is more evident as the notch takes up the more crack-like configuration of the elliptical notch; Figs 7(a) and 8(a).

When $\lambda = 1$, the plastic zone is axisymmetrical and annular for the circular notch (Fig. 3(b)), and symmetry is maintained for the pure shear state, $\lambda = -1$, (Fig. 3(c)), with respect to an axis inclined at 45 degrees to the directions of the applied loads; any slight departure from symmetry is attributable to the irregularity and lack of symmetry of the mesh with respect to this axis. For the circular notch and $\lambda = -1$, yielding first commences at relatively low stress values at the edges of the notch closest to the loading directions, but a plastic enclave also appears on the maximum shear plane some short distance from the notch. When the stress is increased, plasticity rapidly envelops the entire zone shown in Fig. 3(c), except for areas ahead of the plastic localities in which cracks normally initiate. The elliptical notch, i.e., a non-symmetrical hole, exhibits a marked difference in behaviour, and plasticity is more concentrated at the edge of the smallest radius of curvature. For example, compare Figs 3(b) and 6(b).

General yielding occurs at a lower value of σ_p in the shear mode in comparison with the uniaxial mode, which, in turn, requires a lower value of σ_p than the equibiaxial mode.

The stress and strain concentration factors illustrated in Fig. 9 for the three biaxial states and increasing σ_p stress levels, show that the highest concentrations occur in the shear mode and the lowest in the equibiaxial tension mode. Elliptical holes, as would be expected, produce higher concentration factors than the circular holes. Note also the closer grouping in Fig. 9(c) for the ellipse than in Fig. 9(b) for the circle. This is because of the smaller difference in the relative values of the stress concentration factors for the three biaxial loading modes in the case of the ellipse than in the case of the circle; refer to an earlier comment in relation to the data of Table 1.

Cracked notches

Generally, in a cracked notch, the crack tip plastic zones are enhanced due to the effect of the notch concentration field. Also, the stress distributions for the uncracked and cracked notches are different. In the former the maximum stress occurs at the notch root, while in the latter the largest stresses are in the crack

tip region, and the stress at the notch root is low. Because of this, a region near the notch root (which is within the notch plastic enclave when no crack is present) behaves elastically in the cracked notch at the same applied load.

For the uniaxial loading mode (Figs 4(a), 5(a), 7(a), and 8(a) the shapes of the crack tip plastic zones are similar to the ones for the plane crack. In the shear mode (Figs 4(c), 5(c), 7(c), and 8(c)) there is a notch plastic zone far removed from the crack tip plastic zone, in addition to the previously mentioned small plastic zone on the plane of maximum shear stress. All three zones eventually link together as the applied load increases. The patterns for equibiaxial loading are different again, insofar as there is an increasing interaction between, and an eventual linking of, crack tip and notch zones for the circular hole (Fig. 5(b)) but not for the elliptical hole, even for the shorter crack. This will be considered in more detail later.

J *contour integrals*

The J integrals, in general, remained path independent, even when plasticity was widespread at the higher loads. However, in the case of the shorter cracks, there were some occasions when the results from the first two paths were somewhat different from the others. This was probably due to the path traversing some of the large irregularly- and differently-shaped plastically deformed elements. In consequence, the results presented here are for the Γ_3 path shown in Fig. 2, since this path consistently produced a sufficiently reliable representation. The maximum values of J integrals attained in the present study correspond to the loading configuration illustrated in Fig. 5(a), when σ_p equals 280 MPa. The J integral values (in N/mm) are 25.426, 25.239, 25.357, and 25.119, for the first, second, third, and fourth paths, respectively, i.e., the largest difference between them is 1.2 per cent.

Figures 12(a) and 12(b) give, for the circle and the ellipse, respectively, the variation of J/G_N with the applied load, $(\sigma_p/\sigma_{yo})^2$, for different loading situations. They show that, for moderate values of the load, i.e., those values for which the crack tip plastic zone is confined well within the boundaries of the specimen, the values of J corresponding to a given loading mode, λ, remain fairly constant. The ordinate axes correspond to the elastic condition when J is equal to Griffith's energy release rate $G = Y^2 G_N$, where Y is the stress intensity geometry factor. Hence, the intercept on the ordinate axis of the curve for a given configuration and value of λ gives the corresponding value of Y^2. A rapid upward trend of the curve with increasing values of the load indicates that a state of general yield is being approached and, as already mentioned, this occurs at a lower load when $\lambda = -1$ than when $\lambda = 1$ or $\lambda = 0$. Also, the closer grouping of the curves in the case of the elliptical hole, compared with the circular hole, reflects the correspondingly smaller differences between the ratios of the values of Y for the different values of λ; see Table 2.

The elastic T *and* B terms

For a plane crack under SSY conditions, J, G and K_I do not depend on λ, and J varies little from G when the crack tip plastic zone is small. However, the dependence on biaxiality of crack tip field quantities, such as the crack tip plastic zone size, the CTOD and the intensities of plastic deformation in the crack tip region, is well documented (**9**)–(**13**). Therefore, and despite J (or G or K_I) being the most influential crack tip field characterization parameter, a second independent parameter which is sensitive to biaxiality is required; this is provided by the elastic T term (**14**)(**9**). It will be recalled that T is the first non-singular term in Williams' eigenfunction expansion for the asymptotic crack tip stress field (**15**). Since T depends not only on λ, but also on the magnitude of the applied load, namely σ_p and, therefore, K_I, it is usual to normalize T with respect to the stress which would induce a stress intensity K_I at the tip of an Inglis crack of length $2c$ (**16**). The non-dimensional parameter $B = T\sqrt{(\pi c)}/K_I$ is geometry dependent, and also depends on λ. However, for any fixed value of λ, i.e., when the load is applied proportionally, B does not depend on the magnitude of the applied load. For instance, in the case of the Inglis crack, B takes the values -1, 0, -2, corresponding to $\lambda = 0$, 1, -1, respectively, regardless of the values of σ_p or K_I.

When the crack emanates from a notch, B displays the same dependence on geometry and λ, but it is independent of the load, K_I, as in the case of the plane crack. Note, however, that K_I is not independent of λ, because the stress intensity geometry factors are different for different values of λ.

The two independent parameters, K_I (or J) and T (or B) will be used to interpret some of the results of the present analyses.

Crack profiles and crack tip opening

The crack profiles shown in Fig. 10 for cracks of different lengths, emanating from different notch shapes, and subjected to different load levels and loading conditions, reveal that the maximum separation between crack flanks occurs when $\lambda = -1$ and the minimum separation when $\lambda = 1$. Note that these values of λ correspond also to the maximum and minimum values of the stress intensity geometry factors, Y, respectively; see Table 2.

Figures 11(a) and 11(b) give the normalized CTOD, $2000\,v/c$ against J for the circle and the ellipse, respectively. In all cases CTOD is proportional to J, and the constant of proportionality is given by the slope of the linear relationship.

In the case of the circle, the slopes are approximately the same for the different values of λ when $c/a = 1.5$. However, the line for the shorter crack ($c/a = 1.25$) emanating from the elliptical hole is somewhat steeper than the other lines. On the other hand, the relationships for the ellipse in Fig. 11(b) show a marked dependence on λ; the largest slope corresponding to $\lambda = -1$.

The explanation of the different responses for the circle and the ellipse may be found in the values of the crack tip biaxiality parameter, B. Since the CTOD

is dependent on both J and B, it follows that the slope of the linear dependence of CTOD on J must be different for different values of B. From previously quoted work **(1)(3)** the biaxiality effect appears greater for cracks emanating from elliptical holes when compared to circular holes. It seems plausible, therefore, that in the case of the circular hole, which has a large root radius compared to that of the elliptical hole, the values of B are not very different for the different values of λ considered here. On the other hand, in the case of the elliptical hole with the smaller notch root radius, the variation of B with λ is likely to be more pronounced. Preliminary estimates of values of B for the circular and elliptical holes with the longer crack ($c/a = 1.5$) were obtained by using Eshelby's method **(17)(18)**. In the case of the circle, the values of B were found to be very nearly the same (in the region of -0.47) for all the three values of λ. For the ellipse, the values of B were approximately equal to -0.6, -0.2, and -1.0, corresponding to $\lambda = 0$, 1, and -1, respectively. Note also that the largest slope of the CTOD against J curve occurs at the largest negative value of B ($= -1.0$), corresponding to $\lambda = -1$, as expected.

Equivalent plastic strains

Figures 13(a) (for the circle) and 13(b) (for the ellipse) show the variation of the average value of the equivalent plastic strain in the most deformed crack tip element as a function of $(\sigma_p/\sigma_{yo})^2$. As expected, the strains are greatest when $\lambda = -1$ and least when $\lambda = 1$. Note, however, that the values of the equivalent strain are only of qualitative interest, since they are dependent on the mesh size.

Stresses

The major principal stresses at the centres of the elements ahead of the crack tip are shown in Fig. 14(a) for the circle and Fig. 14(b) for the ellipse.

In the linear elastic material, the stress intensity factor determines completely the asymptotic crack tip stress field, but in an elastic–plastic material subjected to loads causing substantial yielding, a number of factors can influence the stresses in the region ahead of the crack, namely:

(a) the elastic stress intensity factor, K_I, which is related to the stress intensity geometry factor, Y, for crack notch configurations;
(b) the material properties, e.g., strain hardening, since this has an effect on the current yield stress;
(c) the elastic T term which affects the hydrostatic component of the stress (For a plane crack in a non-hardening or moderately hardening material, the stresses in the region of the crack tip tend to increase with T and are generally greatest when $\lambda = 1$, and least when $\lambda = -1$; the opposite is true of the strains **(10)(11)**.);
(d) the redistribution of the stresses in an area surrounding the crack tip following the linking up of the notch and the crack tip plastic zone, when the crack tip plastic zone reaches the specimen boundary.

Some of these influences may be illustrated by the present results, but it must be emphasized that the maximum major principal stresses in the crack tip region, emerging from the finite element solutions, are somewhat dependent on mesh size in the immediate vicinity of the crack tip. Here it may be relevant to recall that the Rice–Rosengren–Hutchinson (**19**)(**20**) SSY asymptotic solution for crack tip stress and strain fields in a material obeying power-law hardening, exhibits stress and strain singularities at the tip of the crack. The exception is the degenerate non-hardening case, for which there is no stress singularity and an r^{-1} shear strain singularity. The finite values of the maximum principal stresses are, therefore, of qualitative interest only, but they may, nevertheless, be of help in seeking indications of significant trends when comparing different geometries and loading modes.

As was noted earlier, item (a) above plays a dominant role with regard to the relative values of the stresses corresponding to the different geometries and loading modes. Some of the factors mentioned above can be in conflict with one another, e.g., items (b) and (c), since negative values of T tend to reduce the stresses in the crack tip region on account of (c), while at the same time the increased strains contribute to more strain hardening.

The effect of the hydrostatic component of the stress, item (c), is perhaps noticeable when comparing cases of circular and elliptical holes. These are for the crack length of 4 mm (c/a = 1.5), an applied load σ_p/σ_{yo} of 0.603, but different loading modes; $\lambda = 0$ for the circle and $\lambda = 1$ for the ellipse. In both situations the plasticity is confined to the crack tip regions (see Figs 5(a) and 8(b)). Using the J derived values of the Y factors given in Table 2, the ratio of K_I (circle)/K_I (ellipse) is 1.107 and the ratio J (circle)/J (ellipse) is 1.255. The ratio of the respective values of the maximum equivalent crack tip strains is 1.261, and the ratio of the respective values of principal stresses is 0.952. The higher values of the stresses in the case of the elliptical hole, in spite of the lower value of K_I and the smaller strains, would suggest that this effect is due to item (c) above.

It is more difficult to dissociate the effects of (c) and (d), but compare, for the same crack length of 2 mm and the same loading mode $\lambda = 1$, the circular hole at the load $\sigma_p/\sigma_{yo} = 0.875$ with the elliptical hole at the load $\sigma_p/\sigma_{yo} = 0.739$. The ratio of the respective values of K_I is 1.028, using reference (**1**) Y factors. The ratio of the respective values of maximum major principal stress is 0.912. In view of the shortness of the actual crack, the difference in the influence of the T terms is unlikely to account entirely for the significantly lower stresses in the case of the circular hole compared with the elliptical hole. A possible interpretation is that the lower stresses are attributable to the stress relief caused by the linking up of the notch and the crack tip plastic zone (see Fig. 4(b)).

Again, other things being equal, the largest plastic zone sizes and plastic strains occur in the shear loading mode, $\lambda = -1$. Thus, for the elliptical hole with the shorter crack, at the load $\sigma_p/\sigma_{yo} = 0.603$, the value of the maximum equivalent strain in Fig. 13(b) is approximately three or more times larger when

$\lambda = -1$, in comparison with the other two loading modes. In addition, a glance at Table 2 shows that the stress intensity factor, Y, (and, therefore, K_I) is also larger when $\lambda = -1$ than when $\lambda = 0$ or $\lambda = 1$, but, in spite of the much greater strain hardening, the stresses are lowest for the shear mode, $\lambda = -1$ (see Fig. 14). The fact that the plastic zone covers a large part of the specimen and reaches the boundary in several places as general yield is approached (see Fig. 7(c)) is the most likely cause of the lower stresses.

General comments

If the rate of fatigue crack propagation is related to the intensity of plastic straining in the crack tip region, it would be expected that, for the same value of σ_p, the rate would be fastest for the shear loading mode ($\lambda = -1$) and slowest for the equibiaxial loading mode ($\lambda = 1$). This has indeed been observed in experiments (**4**)(**21**).

When a crack emanating from a hole is subjected to biaxial loading, the effect of biaxiality is felt at a much greater distance than the range suggested by equation (1), which is applicable only to the uniaxial loading mode. This is mainly because the stress intensity geometry factors, Y, differ considerably from mode to mode, even when the actual crack is much longer than the range S in equation (1). This is true for a linear elastic material and, *a fortiori*, for an elastic–plastic material.

Additional studies to determine the elastic T terms corresponding to different geometries, e.g., crack lengths and notch aspect ratios, would be useful. These could be conveniently carried out using Eshelby's method (**17**)(**18**). Further analyses could also be carried out to cover a wider range of aspect ratios and different values of the ratios a/W and H/W.

Finally, future investigations might also consider the effects on cracked notch geometries of mixed mode loading, and different strain hardening laws, e.g., kinematic hardening and cyclic hardening (or softening) with the number of cycles. Three-dimensional studies could also bring benefits in understanding non-through thickness cracks in notched components.

Conclusions

(1) Detailed elastic–plastic finite element analyses of notches with cracks emanating from them can be useful in interpreting fatigue crack propagation under conditions of biaxial loading. Generally, of the three loading modes, the shear loading mode, $\lambda = -1$, results in the largest plastic strains in the region of the crack tip, and the equibiaxial mode, $\lambda = 1$, in the least plastic strains. Hence, at the higher load ranges producing substantial crack tip plastic zones, fatigue crack propagation rates would tend to be fastest when $\lambda = -1$ and slowest when $\lambda = 1$.

(2) Under biaxial loading, the range of action of the notch can be considerably greater than for the uniaxial loading mode.

(3) In an elastic–plastic material, the crack tip stresses are influenced by a number of factors, in addition to the elastic stress intensity factor, K_I, namely, the material properties, the elastic T term, and the interaction of the crack tip plastic zone with the notch plastic zone, or with a specimen boundary, especially when the plasticity is extensive.

Acknowledgement

The author is indebted to Professor K. J. Miller for having suggested and arranged this study and for his very helpful suggestions in the preparation and layout of the paper.

References

(1) XIAO, S. T., BROWN, M. W., and MILLER, K. J. (1985) Stress intensity factors for cracks in notched finite plates subjected to biaxial loading, *Fatigue Fracture Engng Mater. Structures*, **8**, 349–372.
(2) SMITH, R. A., JERRAM, K., and MILLER, K. J. (1974) Experimental and theoretical fatigue-crack propagation lives of variously notched plates, *J. Strain Analysis*, **9**, 61–66.
(3) SMITH, R. A. and MILLER, K. J. (1977) Fatigue cracks at notches, *Int. J. Mech. Sci.*, **19**, 11–22.
(4) YAO, J., BROWN, M. W., and MILLER, K. J. (1985) Development of short cracks at notches in multiaxial fatigue, paper presented at the Second International Conference on Biaxial/Multiaxial Fatigue, Sheffield University, December.
(5) PETERSON, R. E. (1974) *Stress concentration factors*, Wiley, New York.
(6) KFOURI, A. P. and MILLER, K. J. (1974) Stress, displacement, line integral and closure energy determination of crack tip stress intensity factors, *Int. J. Pressure Vessels Piping*, **2**, 179–191.
(7) KFOURI, A. P. and MILLER, K. J. (1976) Crack separation energy rates in elastic plastic fracture mechanics, *Proc. Instn mech. Engrs*, **190**, 571–584.
(8) ISIDA, M. (1971) Effect of width and length on stress intensity factors of internally cracked plates under various boundary conditions, *Int. J. Fracture Mech.*, **7**, 301.
(9) LARSSON, S. G. and CARLSSON, A. J. (1973) Influence of non-singular stress terms and specimen geometry on small scale yielding at crack tips in elastic–plastic materials, *J. Mech. Phys Solids*, **21**, 263–277.
(10) MILLER, K. J. and KFOURI, A. P. (1974) An elastic–plastic finite element analysis of crack tip fields under biaxial loading conditions, *Int. J. Fracture*, **10**, 393–404.
(11) KFOURI, A. P. and MILLER, K. J. (1978) The effect of load biaxiality on the fracture toughness parameters J and G^{Δ}, *Fracture 77. Advances in research on the strength and fracture of materials*, Edited by TAPLIN, D. M. R., Pergamon Press, Oxford, Vol. 3, pp. 241–246.
(12) MILLER, K. J. and KFOURI, A. P. (1977) *A comparison of elastic–plastic fracture parameters in biaxial stress states, ASTM STP 668*, pp. 214–228.
(13) KFOURI, A. P. and MILLER, K. J. (1985) Crack separation energy rates for inclined cracks in a biaxial stress field of an elastic–plastic material, *Multiaxial Fatigue, ASTM STP 853*, Edited by MILLER, K. J. and BROWN, M. W., American Society for Testing and Materials, Philadelphia, PA, pp. 88–107.
(14) RICE, J. R. (1974) Limitations to the small scale yielding approximation for crack tip plasticity, *J. Mech. Phys Solids*, **22**, 17–26.
(15) WILLIAMS, M. L. (1957) On the stress distribution at the base of a stationary crack, *J. appl. Mech.*, **24**, 109–114.
(16) LEEVERS, P. S. and RADON, J. C. (1982) Inherent stress biaxiality in various fracture specimen geometries, *Int. J. Fracture*, **19**, 311–325.
(17) CARDEW, G. E., GOLDTHORPE, M. R., HOWARD, I. C., and KFOURI, A. P. (1985) On the elastic T term, *Fundamentals of deformation and fracture, proceedings of the Eshelby Memorial Symposium*, Edited by BILBY, B. A., MILLER, K. J., and WILLIS, J. R., Cambridge University Press, pp. 465–476.

(18) KFOURI, A. P. (1986) Some evaluations of the elastic T term using Eshelby's method, *Int. J. Fracture*, **30**, 301–315.
(19) RICE, J. R. and ROSENGREN, G. F. (1968) Plane strain deformation near a crack tip in a power-law hardening material, *J. Mech. Phys Solids*, **16**, 1–12.
(20) HUTCHINSON, J. W. (1968) Singular behaviour at the end of a tensile crack in a hardening material, *J. Mech. Phys Solids*, **16**, 13–31.
(21) BROWN, M. W. and MILLER, K. J. (1985) Mode I fatigue crack growth under biaxial stress at room temperature, *Multiaxial fatigue, ASTM STP 853*, Edited by MILLER, K. J. and BROWN, M. W., American Society for Testing and Materials, Philadelphia, pp. 135–152.